


Rashba-like spin-orbit and strain effects in tetragonal PbTiO₃R. Arras,^{1,2,*} J. Gosteau,¹ H. J. Zhao^{⊗,2} C. Paillard^{⊗,2,3} Y. Yang,^{2,4,5,6} and L. Bellaïche²¹*CEMES, Université de Toulouse, CNRS, UPS, 29 Rue Jeanne Marvig, F-31055, Toulouse, France*²*Physics Department and Institute for Nanoscience and Engineering University of Arkansas, Fayetteville, Arkansas 72701, USA*³*Laboratoire SPMS, CentraleSupélec/CNRS UMR8580, Université Paris-Saclay, 8-10 Rue Joliot-Curie, 91190 Gif-sur-Yvette, France*⁴*National Laboratory of Solid State Microstructures, Department of Materials Science and Engineering, Nanjing University, Nanjing 210093, China*⁵*Jiangsu Key Laboratory of Artificial Functional Materials, Nanjing University, Nanjing 210093, China*⁶*Collaborative Innovation Center of Advanced Microstructures, Nanjing 210093, China* (Received 17 September 2019; revised manuscript received 23 October 2019; published 11 November 2019)

We performed first-principles calculations of the spin-orbit effect appearing in the electronic structure of the well-known ferroelectric perovskite oxide PbTiO₃ and analyzed the results within group-theory-derived models. We evidenced some non-negligible linear Rashba spin splittings of the unoccupied *p* bands of Pb atoms and occupied *p* bands of oxygen atoms. Our calculations also show that a cubic spin splitting is present for the unoccupied *d_{xy}* bands of Ti atoms. All these spin-orbit effects lead to complex spin textures reversible by switching the electric polarization, which could be used for future spinorbitronic applications. Our results also demonstrate how applying epitaxial strain could be envisaged to tune these properties by changing the relative energy of some of the bands or the magnitude of the linear/cubic coefficients describing the spin splitting.

DOI: [10.1103/PhysRevB.100.174415](https://doi.org/10.1103/PhysRevB.100.174415)**I. INTRODUCTION**

Spin-orbit effects in nonmagnetic materials lacking inversion symmetry allow a momentum-dependent lifting of band spin degeneracies and the appearance of spin-dependent electronic and transport properties.

Discovered 60 years ago [1–3], spin-orbit effects in nonmagnetic semiconductors were recently suggested as one of the most important research topics in condensed-matter science due to their possible use for spintronic and spinorbitronic applications [4–7]. Proposed some years after the Dresselhaus effect [1], which originates from the so-called bulk inversion asymmetry, the Rashba effect [2,8] is generally related to the presence of a structural inversion asymmetry, linked with a potential asymmetry and a polar axis. Mostly known in two-dimensional electron-gas systems, the Rashba effect offers a way of functionalizing interfaces and surfaces as its strength can be tuned by applying an electric field [9]. The Rashba effect is also known as the key property to design the spin field-effect transistor proposed by Datta and Das in 1990 [4]: In this device, the spin of electrons experiencing a magnetic field due to the Rashba effect in the channel will rotate and acquire a certain state when entering in the drain, which will depend on the applied electric field. More recently, Manipatruni *et al.* [7] proposed an energy-efficient spin-orbit logic device, in which writing operations were performed thanks to ferromagnetic magnetoelectric switching, while the reading was done using spin-to-charge conversion, allowed in nonmagnetic materials, *via* the inverse spin Hall effect or the inverse Edelstein effect [10–14]. The spin-orbit effects could

also be detected and used in innovative devices when taken into account in ferroelectric tunnel junctions, owing to the tunneling anomalous Hall effect [15].

Some years ago, it was found theoretically that the Rashba effect can additionally be present in ferroelectric Rashba semiconductors (FERSC) like GeTe and that the resulting spin textures can be reversed by manipulating the electric polarization [16]. This first prediction was later confirmed experimentally [17,18] and motivated other investigations to propose materials more suitable for applications [19–25].

In their study of BiTeI, Bahramy *et al.* [26] proposed some rules to increase the Rashba parameter γ , considering $\mathbf{k} \cdot \mathbf{p}$ perturbative theory: A higher spin splitting could be obtained by maximizing the spin-orbit strength, minimizing the energy difference between neighboring states, and finally having neighboring states with compatible symmetry character, suggesting we look toward semiconductors with narrow band gaps. Even if a high Rashba spin splitting (RSS) of 4.8 eV Å was obtained with GeTe, its narrow band gap appears in fact to be detrimental to retain the electric polarization and further to control the Rashba-induced spin texture.

Djani *et al.* [25] recently defined additional rules to obtain functional FERSC with high RSS at the bottom of the conduction band and a sustainable electric polarization. They first studied the perovskite WO₃ which presents a heavy 5*d*⁰ element in the octahedral atomic site and an out-of-plane polarization. They found that the lowest bands, with a majoritary *d_{xy}* character, i.e., orbitals lying in the plane perpendicular to the electric polarization, present an almost zero RSS, on the contrary to *d* bands lying above. They further studied Bi₂WO₆ material for which the electric polarization is in plane, while the atomic confinement is out of plane, moving the bottom *d_{xy}* bands upper in energy. For this material, they calculated a

*remi.arras@cemes.fr

Rashba parameter of the order of 1 eV Å and they showed that the electric polarization was also robust with electron doping.

In addition to Bi-based compounds [19,25], lead-based materials also show promising properties in the case of halide perovskites [27,28].

In this paper, we investigate the setting of the Rashba effect in the well-known bulk ferroelectric oxide PbTiO₃. We show that the unoccupied *p* bands of the Pb heavy cation in the A site display a non-negligible *linear* RSS and that the *d*_{xy} bands of the Ti atoms can also possess a large *cubic* spin splitting in some specific HS directions of the first Brillouin zone. Furthermore, the relative position of the *p* and *d* bands can be modified by applying a compressive in-plane strain and the magnitude of the RSS can be tuned.

II. CALCULATION DETAILS

We performed density-functional theory (DFT) calculations by using the VIENNA AB INITIO PACKAGE (VASP) [29,30] with projector-augmented wave [31] pseudopotentials, a cut-off energy of 500 eV, and the generalized gradient approximation for the exchange-correlation energy with the Perdew-Burke-Ernzerhof version revised for solids (GGA-PBESol) [32]. The first Brillouin zone was sampled by a 10 × 10 × 10 Monkhorst-Pack grid [33].

Our calculations have been made with a five-atom perovskite unit cell. We considered the *P4mm* space group, which corresponds to a tetragonal lattice with the electric polarization along the [001] direction. The epitaxial strain is modeled by fixing the in-plane lattice parameter *a* to a certain value and by minimizing the total energy to determine the optimal out-of-plane lattice parameter *c*. All the internal coordinates have been optimized for each structure.

The symmetry analysis and the setup of the *k* · *p* Hamiltonians have been made using the resources from the Bilbao crystallographic server [34,35] and Refs. [36–39].

The spin-orbit interaction, as implemented in VASP [40], was added self-consistently. The linear Rashba coefficient γ can be obtained by the formula $\gamma = \frac{2E_R}{k_R}$, where *k_R* is the shift from the considered high-symmetry (HS) point of the band parabola extremum and *E_R* is the difference of energy between this extremum and the band energy at the same HS point [16,19]. This method can only be used considering a linear Rashba effect. Another method, also valid for higher-order in *k* variation, consists of fitting, around the HS point, the energy difference of the two bands experiencing the spin splitting. To obtain all the coefficients, we used approximately 50–70 *k* vectors, with a maximum norm of 0.04 Å⁻¹ (the norm being calculated according to the HS point taken as the origin).

All the band energies are further given relatively to the Fermi energy *E_F*, which is arbitrarily set at the valence band maximum (VBM).

III. RESULTS

A. General properties of PbTiO₃ bulk

The equilibrium lattice parameters have been calculated to be *a*₀ = 3.881 Å and *c*₀ = 4.156 Å, corresponding to a *c*₀/*a*₀ ratio of 1.071, in agreement with theoretical and experimental data from the literature [41,42].

The calculated band structure without spin-orbit interaction is given in Fig. 1(a), showing an indirect band gap with a width of 1.65 eV, which is lower than the experimental value of 3.4 eV [43] (this underestimation is typical of standard DFT calculations): The VBM is located at the *X* point and has a mixed Pb-*s* and O-*p* character, while the conduction band minimum (CBM) is at the *Z* point, with a Ti-*d*_{xy} character and an energy close to its value at the Γ point. At the *X* point, we can notice a direct band gap of 2.86 eV between the VBM and the *d*_{xz} + *d*_{yz} bands of Ti, the *p*_x + *p*_y bands of Pb being only 0.03 eV above these last ones.

Having spin splittings in a ferroelectric material like PbTiO₃ is interesting as it presents a large band gap, which would allow avoiding charge leakage and altering the electric polarization. Previous calculations have shown that the polar distortion is robust upon hole doping, down to −0.15 |*e*|/formula units (f.u.)—where *e* corresponds to the electric charge of an electron—and even increases by more than 40% in the case of electron doping by adding +0.15 |*e*|/f.u. [44,45]. Moreover, this ferroelectric material presents the advantage to be well known and already widely used for different applications. This material or parent compounds have also been proposed to design future low-energy-consumption heterostructures such as magnetoelectric multiferroic interfaces [46–49] by adding a magnetic electrode. As we will show in the next section, the VBM and the CBM display interesting spin-orbit effects and these bands could be addressed by contacting PbTiO₃ with a suitable metallic electrode. A good choice of metal would ideally have the same cubic structure as PbTiO₃, a small lattice mismatch, and a work function Φ close to the ionization potential (experimentally measured to 6.2 eV [43]) to address the VBM, or close to the electronic affinity (2.8 eV [43]) for the CBM: Some candidates could then be Pd ($\Phi = 5.22$ –5.60 eV [50], *a* = 3.89 Å), Pt ($\Phi = 5.12$ –5.93 eV [50], *a* = 3.92 Å), or Ir ($\Phi = 5.00$ –5.67 eV [50], *a* = 3.84 Å) for the VBM, or Ag ($\Phi = 4.26$ –4.74 eV [50], *a* = 4.08 Å) for the CBM. Confirming these hypotheses would require extended investigations, in particular to address all the specific questions which can arise when dealing with interfaces (preservation of the electric polarization, band alignment, and band bending, etc.) [51,52]. A major concern which can strongly affect the Schottky barrier height at metal/oxide interfaces results from the oxidization of the metallic electrode and the subsequent creation of oxygen vacancies in the oxide. Using metallic oxides can thus be interesting as demonstrated by Chen *et al.* [53], who proposed that RuO₂ ($\Phi = 6.1$ eV [54]) and In₂O₃:Sn ($\Phi = 4.5$ eV [55]) could be used instead, with a preference for respectively hole and electron doping.

B. Effects of the spin-orbit coupling

As shown in Fig. 1(b), including the spin-orbit coupling in the calculations induces several lifting of band degeneracies, which are particularly visible for the *p* bands of the Pb-heavy atom.

The *P4mm* space group of PbTiO₃ is linked to the *C*_{4v} point group. At the $\Gamma(0, 0, 0)$, $Z(0, 0, \frac{1}{2})$, $M(\frac{1}{2}, \frac{1}{2}, 0)$, and $A(\frac{1}{2}, \frac{1}{2}, \frac{1}{2})$ HS points, the little group remains *C*_{4v} and it is possible to write a two-band Hamiltonian, up to the third-order

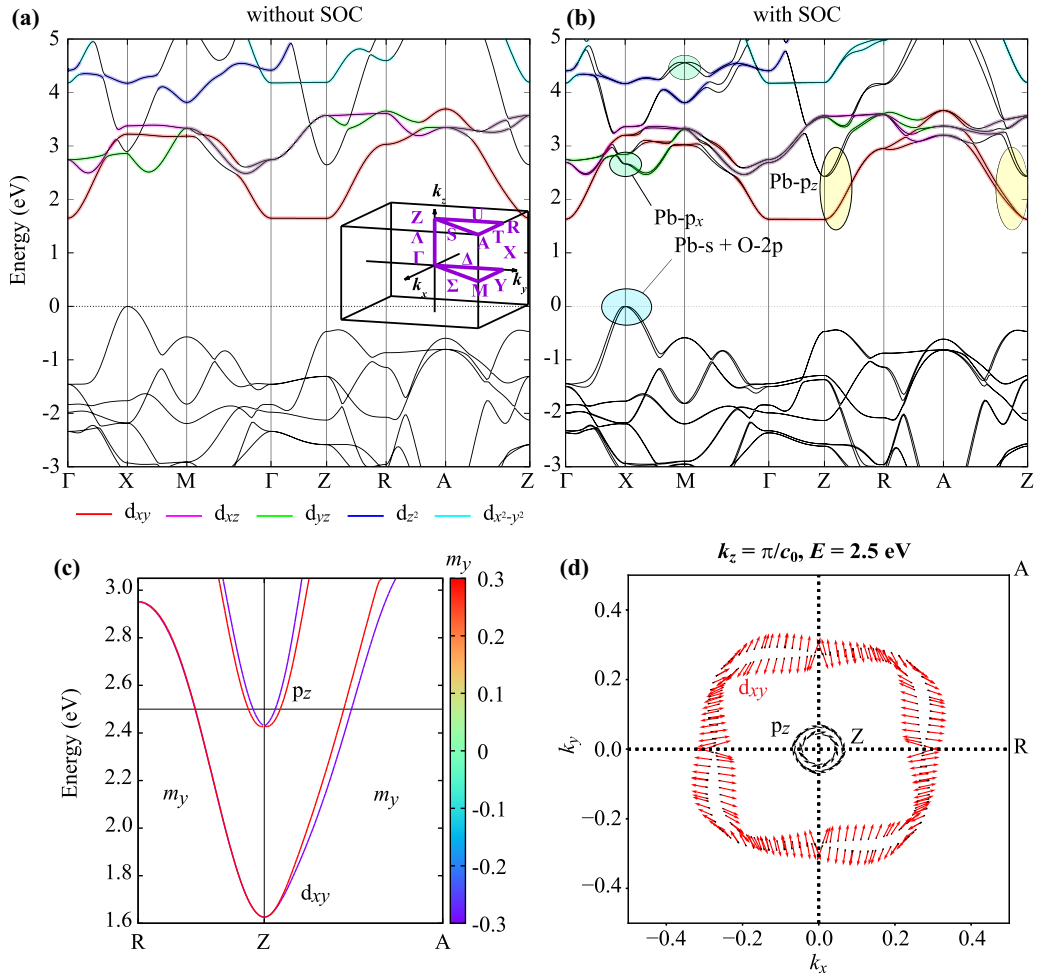


FIG. 1. Band structure of PbTiO₃ (a) without and (b) with the spin-orbit interaction. The majoritarily *d*-orbital contributions are given in color. The origin of the energy is set at the top of the valence bands, which we also consider as the Fermi level. Some areas of interest around the HS points are highlighted. (c) The spin-moment decomposition (in arbitrary units) is given along the full HS lines Z-R and Z-A, to highlight the spin splitting of the yellow area and (d) the corresponding iso-energy ($E = 2.5$ eV) spin texture is given in the Z-R-A plane (for $k_z = \frac{\pi}{c_0}$). The k_x and k_y axis are in units of $\frac{2\pi}{a_0}$.

terms in \mathbf{k} :

$$H_{C_{4v}} = \alpha(k_x^2 + k_y^2) + \beta k_z^2 + \gamma(k_x\sigma_y - k_y\sigma_x) + \gamma'(k_x^3\sigma_y - k_y^3\sigma_x), \quad (1)$$

where k_i ($i = x, y, z$) are the components of the wave vector \mathbf{k} given regarding any HS point taken as the origin, σ_i are the Pauli matrices. α is related to the effective mass m^* by the expression $|\alpha| = \frac{\hbar^2}{2m^*}$ and is given for Pb-*p* and Ti-*d_{xy}* bands in Table I. The term $\gamma(k_x\sigma_y - k_y\sigma_x)$ has the usual form of the linear Rashba effect (γ is thus here the Rashba parameter) [56,57], which will induce a spin splitting in directions perpendicular to Γ -Z. The two other terms which depend on γ' and γ'' are the third-order terms in \mathbf{k} and are in agreement with the derivation made by Vajna *et al.* [56] and Shanavas [58].

In the following, for the sake of simplicity, we will focus our discussion on the CBM bands around the Z HS point shown in Fig. 1(c). Other points will be described only briefly and the special case of the $X(\frac{1}{2}, 0, 0)$ point, which is linked to a C_{2v} little group, is described in Appendix A. We can notice that, according to symmetry considerations, the Hamiltonian

of Eq. (1) only displays terms depending on σ_x and σ_y . Near the HS points, no σ_z -dependent terms are allowed and we

TABLE I. Main parameters of Eqs. (1) and (2) calculated at the HS points for the conduction bands with a mostly Pb-*p* or Ti-*d_{xy}* character and an energy $E - E_F$. The k_{lim} defined in Eq. (3) and calculated in the Γ -M or Z-A directions is also provided to get an idea of the relative effect of the linear (γ) or cubic (γ' and γ'') spin-splitting terms on the band dispersion.

HS Point	$E - E_F$ (eV)	α (m^*) eV \AA^2 (m_0)	γ (eV \AA)	γ' (eV \AA^3)	γ'' (eV \AA^3)	$ k_{\text{lim}} $ \AA^{-1}
Pb- <i>p</i>						
A	5.65	-8.00 (1.35)	0.51	-1.27	-2.82	0.50
Γ	5.46	-4.71 (2.29)	0.93	-3.00	0.87	0.93
M	4.56	-7.98 (1.35)	0.30	2.24	-3.35	0.74
Z	2.43	10.16 (1.06)	0.30	0.92	-2.44	0.63
Ti- <i>d_{xy}</i>						
Γ	1.63	7.25 (1.48)	0.01	-0.87	-0.04	0.15
Z	1.63	6.75 (1.59)	~ 0	7.73	0.11	0.01

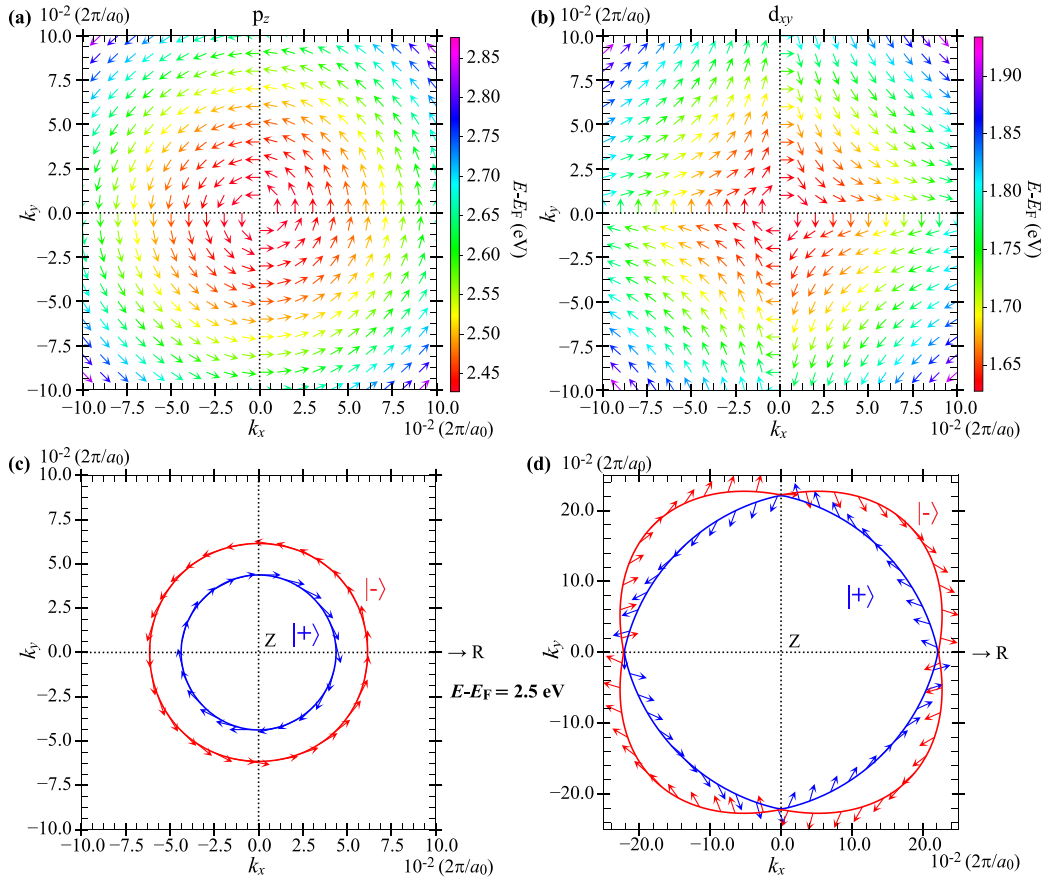


FIG. 2. Spin textures calculated according to the Hamiltonian of Eq. (1) for only one of the two split bands (with only one direction of spin), with (a) a p_z character and (b) a d_{xy} character at the Z point. These spin textures lead to the iso-energy ($E - E_F = 2.5$ eV) spin textures given, respectively, in (c) and (d). The parameters α , γ , γ' , and γ'' used to solve the Hamiltonian are obtained by fitting the band-energy dispersions calculated with the DFT and are given in Table I.

verified from our DFT results that the spin texture has a zero spin magnetization contribution along the $z[001]$ axis for every \mathbf{k} vector.

From the previous Hamiltonian, we can derive the spin-dependent eigenvalues E^\pm to obtain the band-energy dispersions. The difference of these dispersion energies $\Delta E_{C_{4v}} = E^+ - E^-$ for the spin-split bands is defined in the $Z \rightarrow R$ [considering R with coordinates $(\frac{1}{2}, 0, \frac{1}{2})$] and $Z \rightarrow A$ directions as

$$\Delta E_{C_{4v}}(Z \rightarrow R) = 2(\gamma k_x + \gamma'' k_x^3), \quad (2a)$$

$$\Delta E_{C_{4v}}(Z \rightarrow A) = 2\gamma k_{\parallel} + \tilde{\gamma}' k_{\parallel}^3, \quad (2b)$$

with $k_{\parallel} = \sqrt{k_x^2 + k_y^2}$ and $\tilde{\gamma}' = \gamma' + \gamma''$.

We will first consider the RSS of the unoccupied p bands of the Pb atoms. The Pb- p_z bands have an effective mass of $1.06 m_0$ near the Z point (see Table I). As can be observed from Fig. 1(d) (black arrows), these bands also possess an iso-energy spin texture which consists of two concentric circles with tangent spins rotating in inverse directions. The one-band total spin texture is displayed in Fig. 2(a) and is clearly indicative of a linear RSS, as confirmed by our fits of the Pb- p_z bands around the Z HS point, which give an almost isotropic linear-Rashba parameter $\gamma = 0.3$ eV Å.

In Table I, we report the linear Rashba coefficients γ obtained at the other C_{4v} HS points Γ , M , and A for the Pb- p conduction bands. The different spin splittings are generally of the order of 0.30 eV Å but can increase up to 1 eV Å. These higher values remain however lower than the highest values reported in the literature, i.e., 3.8 eV Å for BiTeI [59] or 4.8 eV Å for GeTe [16], for example, even if they are of the same order of magnitude than the splitting reported for a Au(111) surface [60]. They also have the disadvantage to appear at higher energy compared to the Fermi level: from about 4.5 eV at the M point to approximately 5.5 eV at the Γ and A points, compared to 2.43 eV at Z.

The situation for the Pb- p_x bands at the X HS point is more complicated because of its C_{2v} little group and of the proximity of the Ti- d bands (see Appendix A). By comparing Figs. 1(a) and 1(b), we can notice that the Pb- p_x conduction states are split regarding their spin and are lowered in energy when including the spin-orbit interaction, thus appearing as the lowest unoccupied states for this HS point. As discussed in Appendix A, the O- p_x VBM at X also displays a linear anisotropic RSS with an average parameter of $\langle \gamma \rangle = 0.31$ eV Å.

Going back to Figs. 1(c) and 1(d), we can also be interested in considering the d_{xy} bands of the Ti atoms, which are below the p bands of Pb and constitute the CBM. These

bands have some effective mass of $1.59 m_0$ at the Z point, which is nearly four times higher than the calculated values at the $\text{LaAlO}_3/\text{SrTiO}_3$ interface [61]. These bands nonetheless present some spin splitting, which could be compared to the Rashba effect reported in SrTiO_3 [9,58,61,62]. By fitting the band-energy difference as a function of k , we found that, contrary to the p bands, the γ' cubic term is now dominating, partly because of the very low linear term γ . The cubic terms in the spin-splitting Hamiltonian helps introduce an anisotropy as a function of k_{\parallel} in the planes perpendicular to the polar axis, as $\Delta E_{C_{4v}}(Z \rightarrow R)$ does not depend on γ' while $\Delta E_{C_{4v}}(Z \rightarrow A)$ does. We can see that we have a very low spin-splitting in the $Z \rightarrow R$ direction, with a linear Rashba parameter γ of $1 \times 10^{-3} \text{ eV \AA}$ and the cubic term γ'' equal to 0.11 eV \AA^3 . We can thus make the approximation that $\gamma \sim 0$, which gives a purely cubic variation of the spin splitting in the $Z \rightarrow A$ direction, with $\tilde{\gamma}' = 7.84 \text{ eV \AA}^3$, and leading to the one-band spin texture given in Fig. 2(b).

For comparison, we can mention that cubic spin-splitting parameters have been measured or calculated in SrTiO_3 . Nakamura *et al.* [62] deduced from their magnetotransport measurements on $\text{SrTiO}_3(001)$ surfaces a cubic Rashba coefficient of 1 to 2 eV \AA^3 , depending on the carrier density. This experimental value is, however, difficult to compare with our calculations, owing to the fact that in our model, the cubic parameter depends on the considered reciprocal-space direction. The cubic Rashba in SrTiO_3 -based two-dimensional electron systems is generally mostly attributed to the $d_{xz} + d_{yz}$ bands rather than the d_{xy} for which the RSS is rather linear, or even vanishing [58,61,63]: The linear Rashba (when omitting the possibility to have a cubic order) is generally admitted to be of the order of 0.02 eV \AA [9,61] while the cubic parameter has been reported with theoretical values of 4 eV \AA^3 [61] and approximately 2.4 eV \AA^3 [58].

Until now, we said that the $\text{Pb-}p_z$ bands display a spin texture mainly described by its linear term, while the $\text{Ti-}d_{xy}$ bands are on the contrary more related to the cubic terms. It is, however, interesting to note that for the $\text{Pb-}p_z$ bands, the calculated terms γ' and γ'' given in Table I seem to be not negligible, with nonzero values. If we take the energy difference relation of Eqs. (2) in the $Z \rightarrow A$ direction (also valid for $A \rightarrow Z$, $\Gamma \rightarrow M$ and $M \rightarrow \Gamma$ directions), we can define a momentum value above which the contribution of the cubic term $\tilde{\gamma}'$ will start to be higher than the contribution of the linear term:

$$|k_{\text{lim}}(Z \rightarrow A)| = \sqrt{\frac{2|\gamma|}{|\tilde{\gamma}'|}}. \quad (3)$$

The values calculated for $|k_{\text{lim}}|$ at each direction are given in Table I and are really indicative of our observations. Indeed, we can see that they vary from 0.50 to 0.90 \AA^{-1} (i.e., 0.31 to 0.58 in $\frac{2\pi}{a_0}$ units) for the $\text{Pb-}p_z$ bands, which are lengths in the order of the size of the first Brillouin zone, while it is only 0.01 \AA^{-1} (0.01 in $\frac{2\pi}{a_0}$ units) for the $\text{Ti-}d_{xy}$ bands.

If we made the approximation that the spin splitting for the $\text{Pb-}p_z$ bands only depends on γ , and those of the $\text{Ti-}d_{xy}$ bands

only on γ' , then the spin texture would have a form described by the following equations:

$$(m_x^{\pm}, m_y^{\pm})_{\gamma} = \left(\mp \frac{\sin(\theta)}{2}, \pm \frac{\cos(\theta)}{2} \right), \quad (4a)$$

$$(m_x^{\pm}, m_y^{\pm})_{\gamma'} = \left(\mp h(\theta) \frac{\cos(\theta)}{2}, \pm h(\theta) \frac{\sin(\theta)}{2} \right), \quad (4b)$$

where θ is the angle between k_{\parallel} and k_x . $h(\theta) = 1$ if $0 < \theta < \frac{\pi}{2}$ and $\pi < \theta < \frac{3\pi}{2}$ and $h(\theta) = -1$ if $\frac{\pi}{2} < \theta < \pi$ and $\frac{3\pi}{2} < \theta < 2\pi$. The spin magnetization is defined according to its in-plane components $m_i^{\pm} = (\pm|\frac{\sigma_i}{2}| \pm)$ ($i = x, y$), where $|+)$ and $| -)$ are the spin-dependent eigenvectors of the Hamiltonian of Eq. (1).

Equations (4) predict that the spin texture of the p_z bands would consist of spins rotating around the Z point. The bands d_{xy} , if their spin splitting depended only on γ' , would on the contrary have a spin texture made by spin rotating around the corner of the 2D Brillouin zone A, and with no defined value along the Z - R axis. These two approximations agree rather well with the spin textures of Fig. 2. In the case of the d_{xy} bands [Fig. 2(b)], we can observe some spins with a direction perpendicular to the Z - R axis, which are allowed if we take the complete expression for the spin texture, i.e., including the three γ , γ' , and γ'' terms. These perpendicular spins explain the nonzero m_y contribution plotted in Fig. 1(c) for the Z - R direction. Taking simultaneously the spin textures for the two directions of spin ($|+)$ and $| -)$ and at the specific energy $E - E_F = 2.5 \text{ eV}$ allows us to recover approximately the iso-energy spin texture for the p_z [Fig. 2(c)] and d_{xy} [Fig. 2(d)] bands. Combining these two figures gives a result comparable to the DFT texture of Fig. 1(d).

The whole spin textures presented in this paper and extracted from the DFT calculations can, however, be a little more complex than those obtained from our model Hamiltonian, especially those given in Appendices A and B. Different aspects have to be kept in mind. First of all, the given Hamiltonians are defined perturbatively and are only valid *near* the HS points. Second, higher-order terms in k can still be considered, and their magnitudes are expected to increase relatively to the linear term when increasing k , i.e., when going away from the HS points. Finally, a two-band Hamiltonian omits different terms and can be insufficient to describe a system where several bands with different characters are close in energy and hybridize one with each other.

In the previous section, we also mentioned that the electric polarization is persistent upon charge doping. As a first approximation, we have considered that such doping does not change considerably the band structure, and that the change of the Fermi energy is linked with a rigid shift of the whole band structure. A verification of this approximation is beyond the scope of this paper.

If the correct magnitude of each spin splitting parameter is not easy to evaluate with great precision, we, however, verified that the rotation directions of the spins are reversible by switching the electric polarization for all the spin textures presented in this section and in the Appendices.

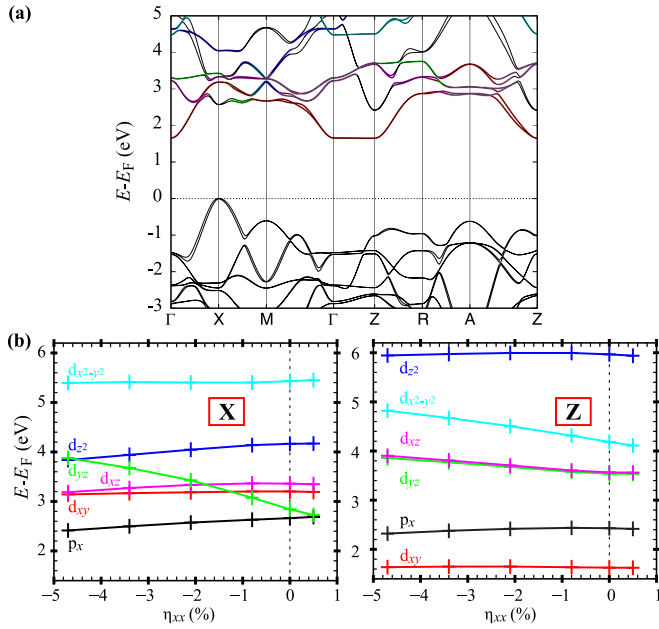


FIG. 3. (a) Band structure of strained PbTiO₃ with spin-orbit interaction, for an in-plane lattice parameter $a = 3.8 \text{ \AA}$. (b) Evolution as a function of the strain η_{xx} of the lowest unoccupied band energies at the X (left panel) and Z (right panel) high-symmetry points.

C. Effects of the strain

We showed the interest of both the p bands of Pb atoms and d bands of Ti for the relatively high linear or cubic spin splittings they can display. It could thus be interesting to be able to tune the energy of these bands to be more or less addressable when PTO is contacted with a metallic layer, and the corresponding spin-splitting magnitude to get different spin textures and transport properties from the same material.

This tunability could be achieved by applying a compressive in-plane strain on PbTiO₃. The $P4mm$ phase of this oxide has been found to be stable for a wide range of in-plane strain η_{xx} , from -7.0% to $+1.3\%$ [64,65]. We define $\eta_{xx} = \frac{a(\text{Sub}) - a_0(\text{PTO})}{a_0(\text{PTO})}$, with $a(\text{Sub})$ being the lattice parameter of a selected substrate and $a_0(\text{PTO})$ the equilibrium in-plane lattice parameter calculated for PbTiO₃. Strain can affect the band structure of semiconductors by, e.g., (i) shifting bands, (ii) tuning band gaps and effective mass of carriers, and even (iii) introducing new band splittings [39]. The first two effects (i) and (ii) are general consequences of strain, while item (iii) only occurs if strain modifies the crystal symmetry [66]. In our investigated PTO materials, only the in-plane biaxial strain ($\eta_{xx} = \eta_{yy}$) and the resulting out-of-plane strain (η_{zz}) can change their values, implying that the $P4mm$ symmetry of PTO is conserved and therefore no new splitting can happen due to this strain application.

In the band structure of Fig. 3(a), which corresponds to an in-plane lattice parameter of 3.8 \AA ($\eta_{xx} = -2.1\%$), and which could be obtained by growing PbTiO₃ on a substrate like LaAlO₃ ($a = 3.789 \text{ \AA}$), we can see that the d_{yz} bands of the Ti atom are shifted upward in energy and the $p_x + p_y$ unoccupied bands are the lowest unoccupied bands at the X point, even if they remain higher in energy than the d_{xy} bands at the Γ and Z points, for which the energy almost

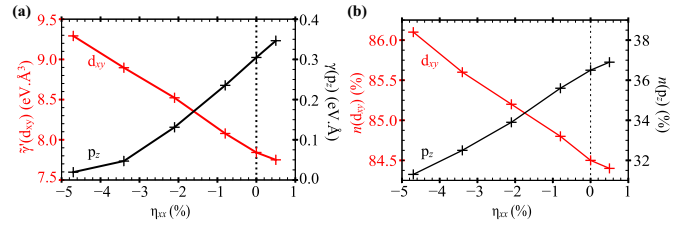


FIG. 4. Evolution as a function of the in-plane strain η_{xx} of (a) the Rashba parameter and (b) the band character n . The results are given for the Ti- d_{xy} (in red) and the Pb- p_z (in black) bands at the Z point.

does not change. This tendency is confirmed if we perform systematic calculations by applying a compressive in-plane strain to PbTiO₃ in the range of $\eta_{xx} = -4.7\%$ to $+0.5\%$ (the calculated out-of-plane lattice parameters and the resulting change of electric polarization P are given in Appendix C). The complete variation of each band energy can be seen in Fig. 3(b) as a function of the in-plane strain, showing that the relative order of the bands stays the same at the Z point, contrary to the X point, which is mainly affected by the strong variation of the d_{yz} bands. With a very large in-plane strain, it could be possible to decorrelate the unoccupied p bands of the heavy atom and the d bands of the transition metal. We have found it is indeed the case for another lone-pair ferroelectric oxide, with a naturally high c/a ratio: BiScO₃ (see Appendix D) possesses Sc- d bands higher in energy than the Bi- p bands and gives Rashba effects similar to those already observed in BiAlO₃ [19].

Focusing on the band splitting at the Z point, Fig. 4(a) shows that the crystal distortion upon in-plane strain affects the Rashba parameter: We observe a linear increase (decrease) as a function of η_{xx} with a coefficient of 7.74 eV \AA (-30.27 eV \AA^3) for the unoccupied Pb- p_z (Ti- d_{xy}) bands. For the Pb- p_z bands, the averaged linear Rashba coefficient is consequently strongly reduced from almost 0.35 eV \AA to nearly 0.02 eV \AA when the lattice parameter is strained down to $\eta_{xx} = -4.7\%$, while on the contrary $\tilde{\gamma}'$ increases from 7.84 eV \AA^3 to 9.29 eV \AA^3 .

From the group theory, considering the strain effect, we can demonstrate this linear variation. It is indeed possible to show that each coefficient ($\alpha, \beta, \gamma \dots$) can be rewritten following the same form,

$$\tilde{\gamma} = \gamma + \gamma_1(\eta_{xx} + \eta_{yy}) + \gamma_2\eta_{zz}, \quad (5)$$

with η_{ij} being the ij elements of the strain tensor in Voigt notation, $\eta_{xx} = \eta_{yy}$, and $\eta_{zz} = -\frac{2C_{12}}{C_{11}}\eta_{xx}$. We can then write

$$\tilde{\gamma} = \gamma + \tilde{\gamma}_1\eta_{xx}, \quad (6)$$

with $\tilde{\gamma}_1 = 2(\gamma_1 - \frac{C_{12}}{C_{11}}\gamma_2)$.

Such formula thus naturally explains the linear dependence with strain of some aforementioned Rashba coefficients.

A more detailed analysis would be necessary to obtain a more complete picture of the Rashba-coefficients variation, in particular for lattice parameters close to the equilibrium. A direct interpretation of the role of the band hybridization and of the interband interactions requires more extensive calculations via, for example, tight-binding models [25,58], which

is beyond the scope of this paper. The Rashba parameter has been predicted to depend on the band-gap energies between bands for which the symmetry allows the perturbative transition [26], and also on the hopping parameters [61], which can be related to the band hybridization. If we consider Fig. 4(b), we can see that a correlation between the evolution of the band character n (obtained after projecting the wave functions onto spherical harmonics in atomic spheres) and those of the spin-splitting parameters could exist. We indeed observe an increase of γ' by nearly 18.5% when η_{xx} goes from 0 to 4.7%, which is concomitant with an increase of 1.9% of the d_{xy} band character for the Ti atoms, which could be linked to a change of the band hybridization and/or a stronger localization of the d_{xy} states in the atomic sphere when reducing the in-plane lattice parameter. For the linear Rashba parameter of the Pb- p_z orbitals, we have on the contrary a strong decrease of γ by 94%, which could be associated with the decrease of $n(p_z)$ by 14%.

In this paper, we chose to focus only on the simplest tetragonal $P4mm$ phase of PbTiO_3 . Other phases (monoclinic or orthorhombic) with an in-plane electric polarization have also been found to be stable for sufficient in-plane tensile strain [64,65]. These phases would thus be interesting as they could promote spin textures with a m_z component. Having a tensile strain would also certainly allow us to decrease the energy of the d_{xz} and d_{yz} bands, which are known to be responsible for inducing a cubic Rashba effect in SrTiO_3 [58,61,63].

IV. CONCLUSIONS

We have analyzed the spin-splitting resulting from the spin-orbit interaction for the highest occupied and lowest

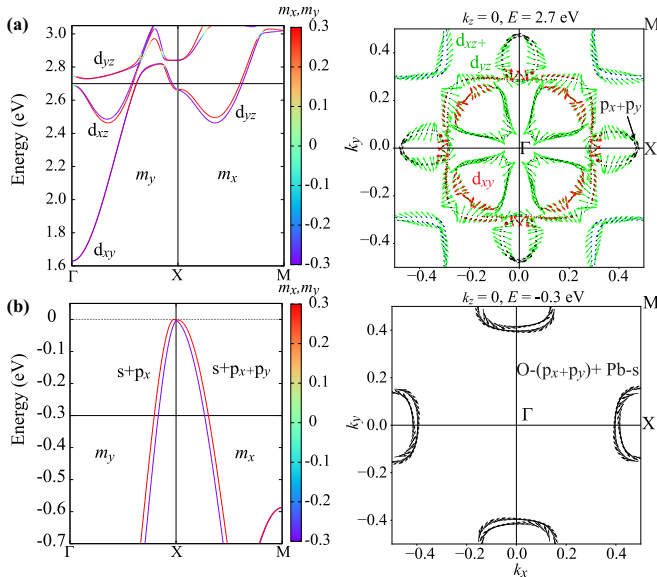


FIG. 5. Spin-projected band structures, with the corresponding iso-energy spin textures for (a) the lowest unoccupied and (b) highest occupied bands. The spin projection for the band structures is done on m_y along X - Γ direction and m_x along the X - M direction, because only k_x or k_y are, respectively, varying along these directions. The iso-energy spin textures are plotted in the Γ - X - M plane (for $k_z = 0$) and for energies $E - E_F = 2.7$ eV and -0.3 eV.

unoccupied bands of the tetragonal and ferroelectric oxide PbTiO_3 . We have shown that the unoccupied p bands of Pb atoms of PbTiO_3 and occupied p bands of oxygen atoms present a non-negligible linear RSS at different HS points of the first Brillouin zone such as the X or Z point, where they are the closest from the Fermi level, with a linear Rashba coefficient of approximately 0.3 eV \AA . The unoccupied Ti- d bands, which constitute the CBM, also display different spin splitting, the variation of which is dominated by cubic terms as a function of the wave vector \mathbf{k} .

The whole spin textures resulting on the combined spin splitting of each band are all reversible by switching the electric polarization direction, but they are quite complex due to the anisotropy induced by the cubic terms, by the symmetry breaking at some HS point or by the contribution of several bands at some energies. Applying a compressive in-plane strain could help promote the contribution of the desired cubic or linear terms of one band or another by changing both the magnitude of the spin-splitting parameters or the relative energies of each band, which will then be able or not to participate to the transport processes.

ACKNOWLEDGMENTS

The authors want to thank M. Bibes and A. Zunger for useful discussions. This study has been partially supported through the EUR Grant NanoX No. ANR-17-EURE-0009 in the framework of the Programme des Investissements d'Avenir. H.J. and L.B. thank the Department of Energy, Office of Basic Energy Sciences, under Award No. DE-SC0002220. C.P. acknowledges ARO Grant No. W911NF-16-1-0227. Y.Y. acknowledges the National Natural Science Foundation of China (Contract No. 11874207). This work was granted access to the HPC resources of CALMIP (Allocation No. 2019/P1229).

APPENDIX A: SPIN TEXTURE IN THE Γ - X - M PLANE

Figures 5(a) and 5(b) give the spin-projected band structure and some iso-energy spin textures around the X HS point for both the lowest unoccupied bands and the VBM. Due to the C_{2v} little group of X point, the difference of energies makes an anisotropic spin splitting appear in the \mathbf{k} space, even if

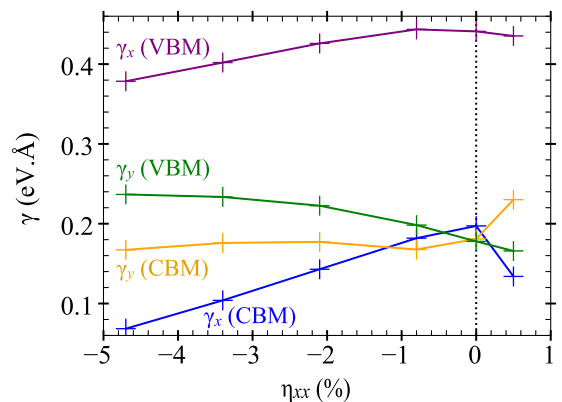


FIG. 6. Variation of the linear Rashba parameters γ_x and γ_y as a function of the in-plane strain η_{xx} around the X point.

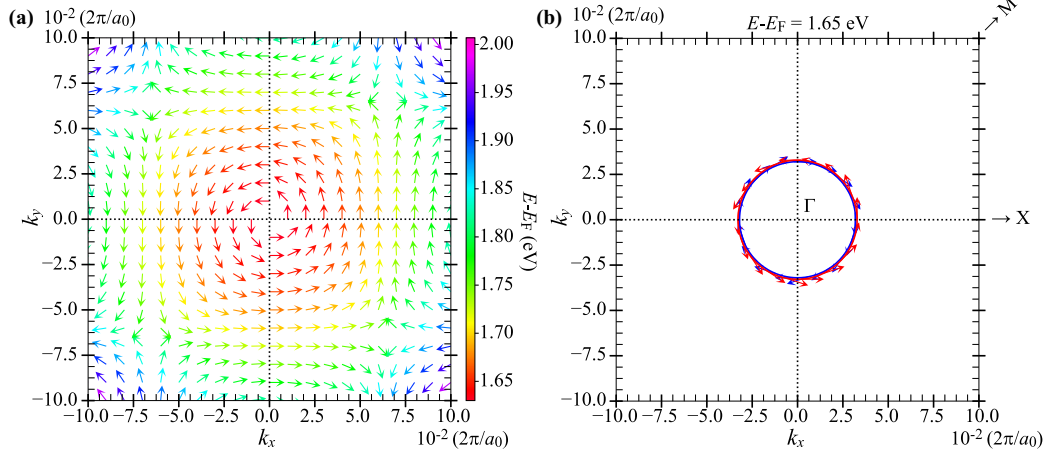


FIG. 7. (a) One-band spin texture calculated from the Hamiltonian of Eq. (1) by using the parameters of Table I for the d_{xy} bands around Γ point and (b) the corresponding iso-energy spin texture ($E = 1.65$ eV) in the Γ - X - M plane (for $k_z = 0$).

considering only first-order terms in \mathbf{k} :

$$\Delta E_{C_{2v}} = 2\sqrt{(\gamma_x k_x)^2 + (\gamma_y k_y)^2}. \quad (\text{A1})$$

The spin texture of the VBM shows the linear RSS made by states with a mostly $O - 2p_x$ character, slightly hybridized with Pb- s states. Unlike for the Pb- p_z states at the Z point and presented in Fig. 1(d), we can see that the circular contours are not exactly isotropic. This is reflected by the two different Rashba coefficients calculated to be $\gamma_x = 0.44$ eV \AA in the $X_{\rightarrow\Gamma}$ direction and $\gamma_y = 0.19$ eV \AA for the $X_{\rightarrow M}$ direction. The unoccupied Pb- p_x states are found less anisotropic ($\gamma_x = 0.20$ eV \AA and $\gamma_y = 0.19$ eV \AA) but the complexity of their corresponding spin texture resides in the energy proximity of the Ti- d_{yz} bands. As seen in Fig. 3(b), these d_{yz} bands can be shifted upward in energy by applying an in-plane strain, which could help to explain the different variations observed for γ_x and γ_y as a function of η_{xx} (see Fig. 6).

For the VBM (/lowest unoccupied bands) along $X_{\rightarrow\Gamma}$, γ_x decreases from 0.44 eV \AA (respectively, 0.19 eV \AA) to 0.38 eV \AA (respectively, 0.07 eV \AA) when decreasing a from 3.9 ($\eta_{xx} = +0.5\%$) to 3.7 \AA ($\eta_{xx} = -4.7\%$). The Rashba coefficient γ_y shows, on the contrary, an increase of approximately 40% in the $X_{\rightarrow M}$ direction for the VBM, from 0.17 to 0.24 eV \AA . It is also noteworthy that the variation of the RSS as a

function of the in-plane lattice parameter is linear in the range of $\eta_{xx} = -4.7\%$ to -0.8% at the X point (Fig. 6), with an increase rate of γ_x 2.92 eV \AA and 1.68 eV \AA , respectively, for the CBM and VBM in the $X_{\rightarrow\Gamma}$ direction. Above $\eta_{xx} = -0.8\%$, the sudden increase of γ_y for the unoccupied Pb- p_x bands (yellow curve) is certainly a result of the crossing with the d_{yz} bands.

APPENDIX B: SPIN TEXTURE AT THE Γ POINT

We described previously the spin splitting and spin textures of the Pb- p_z or Ti- d_{xy} bands at the Z point, where we demonstrated that the behavior is mostly dependent either on γ or γ' . However, if we consider the d_{xy} bands at Γ , we can see from the values of Table I, that $|k_{\text{lim}}|$ is equal to 0.15\AA^{-1} , which corresponds to 0.09 in $\frac{2\pi}{a_0}$ units. We thus expect competition between the linear and cubic spin-splitting terms in the vicinity of the Γ point. In Fig. 7(a), we can see that for $k_x < 0.05$, we have a linear Rashba-like behavior, which can give iso-energy spin textures [Fig. 7(b)] consistent with the DFT calculations, while for $k_x > 0.05$ the spin texture becomes more complex and the model less accurately matches the DFT results (not shown). Despite the discrepancies appearing between the DFT calculations and our model for this spin texture, the band dispersion energies are on the contrary

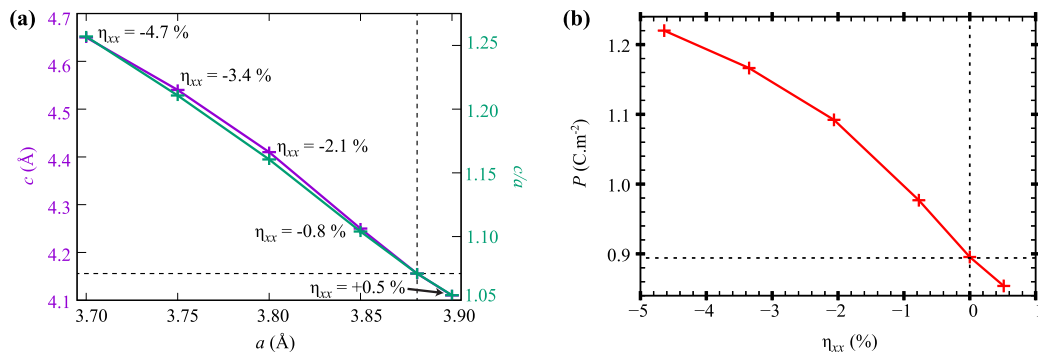


FIG. 8. (a) Calculated out-of-plane lattice parameter c and c/a ratio as a function of the in-plane lattice parameter a . (b) Electrical polarization P as a function of the in-plane strain η_{xx} .

correctly fitted. This shows that, as mentioned at the end of Sec. III B, the model for the spin texture may be mostly valid for \mathbf{k} vectors close to the HS points, i.e., $k_x < 0.05$ in the present case.

APPENDIX C: TETRAGONAL DISTORTION UNDER STRAIN

Decreasing the in-plane lattice parameter a from 3.9 to 3.7 Å increases accordingly the c/a ratio from 1.054 to 1.257, i.e., by $\approx 19\%$, as it can be seen in Fig. 8(a).

The value of the electric polarization P for the equilibrium lattice parameters ($\eta_{xx} = 0$) was estimated to be 0.89 C m^{-2} , from calculations using the Berry-phase formalism [67]. This value is in agreement, even if a little higher, with experimental (0.75 C m^{-2}) [68] and theoretical (0.79 C m^{-2}) [64] values reported in the literature. We then calculated an increase of P as a function of the in-plane strain η_{xx} [see Fig. 8(b)], reaching a value of 1.22 C m^{-2} for $\eta_{xx} = -4.7\%$. Such strain-induced enhancement of polarization is well known in the literature [64].

APPENDIX D: BAND STRUCTURE OF BiScO₃

Figure 9 displays the band structure calculated for tetragonal BiScO₃ ($a = 3.807 \text{ Å}$ and $c = 4.894 \text{ Å}$), which has already been predicted to possess an axial ratio $c/a = 1.285$

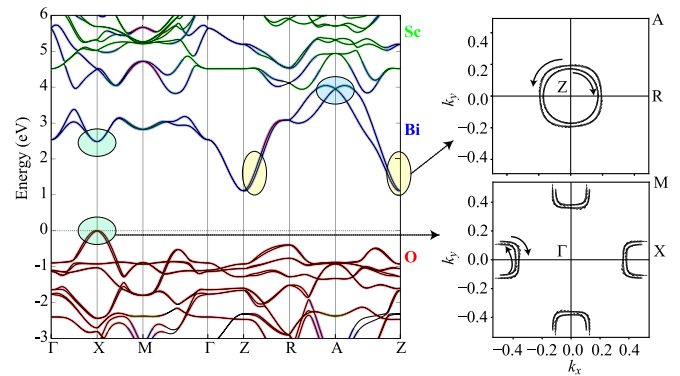


FIG. 9. Band structure calculated for BiScO₃ with the contribution of each atom in color and two spin textures calculated in a $(k_x, k_y, 0)$ plane, to highlight the spin splittings of the VBM at the X point and the CBM at the Z point.

[69]. The band structure gives an indirect band gap of 1.26 eV, with a Bi- p character for the lowest conduction bands. Different spin splittings can be noticed in the vicinity of the HS points. These linear RSS mainly correspond to Rashba parameters of approximately 0.4 eV Å in the vicinity of Z, i.e., for $k_z = \pi/c$, while they are well lower, with values of $0.06\text{--}0.08 \text{ eV Å}$ near Γ and X, for $k_z = 0$.

- [1] G. Dresselhaus, *Phys. Rev.* **100**, 580 (1955).
- [2] E. I. Rashba and V. I. Sheka, *Fiz. Tverd. Tela: Collected Papers* **2**, 62 (1959).
- [3] G. Bihlmayer, O. Rader, and R. Winkler, *New J. Phys.* **17**, 050202 (2015).
- [4] S. Datta and B. Das, *Appl. Phys. Lett.* **56**, 665 (1990).
- [5] D. Bercioux and P. Lucignano, *Rep. Prog. Phys.* **78**, 106001 (2015).
- [6] A. Manchon, H. C. Koo, J. Nitta, S. M. Frolov, and R. A. Duine, *Nat. Mater.* **14**, 871 (2015).
- [7] S. Manipatruni, D. E. Nikonov, C.-C. Lin, T. A. Gosavi, H. Liu, B. Prasad, Y.-L. Huang, E. Bonturim, R. Ramesh, and I. A. Young, *Nature* **565**, 35 (2019).
- [8] Yu. A. Bychkov and É. I. Rashba, *Pis'ma Zh. Eksp. Teor. Fiz.* **39**, 66 (1984) [*JETP Lett.* **39**, 78 (1984)].
- [9] A. D. Caviglia, M. Gabay, S. Gariglio, N. Reyren, C. Cancellieri, and J.-M. Triscone, *Phys. Rev. Lett.* **104**, 126803 (2010).
- [10] V. M. Edelstein, *Solid State Commun.* **73**, 233 (1990).
- [11] J. C. R. Sánchez, L. Vila, G. Desfonds, S. Gambarelli, J. P. Attané, J. M. De Teresa, C. Magén, and A. Fert, *Nat. Commun.* **4**, 2944 (2013).
- [12] S. Bhattacharjee, S. Singh, D. Wang, M. Viret, and L. Bellaiche, *J. Phys.: Condens. Matter* **26**, 315008 (2014).
- [13] E. Lesne, Y. Fu, S. Oyarzun, J. C. Rojas-Sánchez, D. C. Vaz, H. Naganuma, G. Sicoli, J.-P. Attané, M. Jamet, E. Jacquet, J.-M. George, A. Barthélémy, H. Jaffrès, A. Fert, M. Bibes, and L. Vila, *Nat. Mater.* **15**, 1261 (2016).
- [14] W. Han, Y. Otani, and S. Maekawa, *npj Quantum Mater.* **3**, 27 (2018).
- [15] M. Y. Zhuravlev, A. Alexandrov, L. L. Tao, and E. Y. Tsymlal, *Appl. Phys. Lett.* **113**, 172405 (2018).
- [16] D. D. Sante, P. Barone, R. Bertacco, and S. Picozzi, *Adv. Mater.* **25**, 509 (2013).
- [17] M. Liebmann, C. Rinaldi, D. D. Sante, J. Kellner, C. Pauly, R. N. Wang, J. E. Boschker, A. Giussani, S. Bertoli, M. Cantoni, L. Baldrati, M. Asa, I. Vobornik, G. Panaccione, D. Marchenko, J. Sánchez-Barriga, O. Rader, R. Calarco, S. Picozzi, R. Bertacco, and M. Morgenstern, *Adv. Mater.* **28**, 560 (2016).
- [18] C. Rinaldi, S. Varotto, M. Asa, J. Sławińska, J. Fujii, G. Vinai, S. Cecchi, D. Di Sante, R. Calarco, I. Vobornik, G. Panaccione, S. Picozzi, and R. Bertacco, *Nano Lett.* **18**, 2751 (2018).
- [19] Luiz Gustavo Davanse da Silveira, P. Barone, and S. Picozzi, *Phys. Rev. B* **93**, 245159 (2016).
- [20] D. Di Sante, P. Barone, A. Stroppa, K. F. Garrity, D. Vanderbilt, and S. Picozzi, *Phys. Rev. Lett.* **117**, 076401 (2016).
- [21] L. L. Tao and J. Wang, *J. Appl. Phys.* **120**, 234101 (2016).
- [22] L. L. Tao, T. R. Paudel, A. A. Kovalev, and E. Y. Tsymlal, *Phys. Rev. B* **95**, 245141 (2017).
- [23] L. L. Tao and E. Y. Tsymlal, *Nat. Commun.* **9**, 2763 (2018).
- [24] J. Varignon, J. Santamaria, and M. Bibes, *Phys. Rev. Lett.* **122**, 116401 (2019).
- [25] H. Djani, A. C. Garcia-Castro, W.-Y. Tong, P. Barone, E. Bousquet, S. Picozzi, and P. Ghosez, *npj Quantum Mater.* **4**, 51 (2019).
- [26] M. S. Bahramy, R. Arita, and N. Nagaosa, *Phys. Rev. B* **84**, 041202(R) (2011).
- [27] M. Kepenekian and J. Even, *J. Phys. Chem. Lett.* **8**, 3362 (2017).

- [28] S. D. Stranks and P. Plochocka, *Nat. Mater.* **17**, 381 (2018).
- [29] G. Kresse and J. Hafner, *Phys. Rev. B* **49**, 14251 (1994).
- [30] G. Kresse and J. Furthmüller, *Phys. Rev. B* **54**, 11169 (1996).
- [31] P. E. Blöchl, *Phys. Rev. B* **50**, 17953 (1994).
- [32] G. I. Csonka, J. P. Perdew, A. Ruzsinszky, P. H. T. Philipsen, S. Lebègue, J. Paier, O. A. Vydrov, and J. G. Ángyán, *Phys. Rev. B* **79**, 155107 (2009).
- [33] H. J. Monkhorst and J. D. Pack, *Phys. Rev. B* **13**, 5188 (1976).
- [34] M. I. Aroyo, A. Kirov, C. Capillas, J. M. Perez-Mato, and H. Wondratschek, *Acta Crystallogr. Sect. A* **62**, 115 (2006).
- [35] M. I. Aroyo, J. M. Perez-Mato, C. Capillas, E. Kroumova, S. Ivantchev, G. Madariaga, A. Kirov, and H. Wondratschek, *Z. Kristallogr. Cryst. Mater.* **221**, 15 (2009).
- [36] G. F. Koster, J. D. Dimmock, R. G. Wheeler, and H. Statz, in *Properties of the Thirty-Two Point Groups*, edited by G. F. Koster (M.I.T. Press, Cambridge, MA, 1963).
- [37] S. L. Altmann and P. Herzig, *Point-Group Theory Tables* (Clarendon Press, Oxford; Oxford University Press, New York, 1994).
- [38] R. Winkler, *Spin–Orbit Coupling Effects in Two-Dimensional Electron and Hole Systems* (Springer, Berlin, 2003).
- [39] L. C. Lew Yan Voon and W. M., *The $k \cdot p$ Method* (Springer-Verlag, Berlin, 2009).
- [40] S. Steiner, S. Khmelevskiy, M. Marsmann, and G. Kresse, *Phys. Rev. B* **93**, 224425 (2016).
- [41] S. A. Mabud and A. M. Glazer, *J. Appl. Crystallogr.* **12**, 49 (1979).
- [42] T. Shimada, T. Ueda, J. Wang, and T. Kitamura, *Phys. Rev. B* **87**, 174111 (2013).
- [43] R. Schafrank, S. Li, F. Chen, W. Wu, and A. Klein, *Phys. Rev. B* **84**, 045317 (2011).
- [44] H. J. Zhao, A. Filippetti, C. Escorihuela-Sayalero, P. Delugas, E. Canadell, L. Bellaiche, V. Fiorentini, and J. Íñiguez, *Phys. Rev. B* **97**, 054107 (2018).
- [45] C. Paillard, E. Torun, L. Wirtz, J. Íñiguez, and L. Bellaiche, *Phys. Rev. Lett.* **123**, 087601 (2019).
- [46] M. Fechner, I. V. Maznichenko, S. Ostanin, A. Ernst, J. Henk, P. Bruno, and I. Mertig, *Phys. Rev. B* **78**, 212406 (2008).
- [47] V. S. Borisov, S. Ostanin, I. V. Maznichenko, A. Ernst, and I. Mertig, *Phys. Rev. B* **89**, 054436 (2014).
- [48] A. Quindeau, V. Borisov, I. Fina, S. Ostanin, E. Pippel, I. Mertig, D. Hesse, and M. Alexe, *Phys. Rev. B* **92**, 035130 (2015).
- [49] R. Arras and S. Cherifi-Hertel, *ACS Appl. Mater. Interfaces* **11**, 34399 (2019).
- [50] *CRC Handbook of Chemistry and Physics*, internet version (CRC Press, Boca Raton, FL, 2005), pp. 12–124.
- [51] Y. Umeno, B. Meyer, C. Elsässer, and P. Gumbsch, *Phys. Rev. B* **74**, 060101(R) (2006).
- [52] V. Pankoke and S. Gemming, *Eur. Phys. J. B* **67**, 57 (2009).
- [53] F. Chen, R. Schafrank, S. Li, W. B. Wu, and A. Klein, *J. Phys. D* **43**, 295301 (2010).
- [54] R. Schafrank, J. Schaffner, and A. Klein, *J. Eur. Ceram. Soc.* **30**, 187 (2010), Electroceramics XI Special Issue.
- [55] Y. Gassenbauer, R. Schafrank, A. Klein, S. Zafeirotos, M. Hävecker, A. Knop-Gericke, and R. Schlögl, *Phys. Rev. B* **73**, 245312 (2006).
- [56] S. Vajna, E. Simon, A. Szilva, K. Palotas, B. Ujfalussy, and L. Szunyogh, *Phys. Rev. B* **85**, 075404 (2012).
- [57] S. D. Ganichev and L. E. Golub, *Phys. Status Solidi B* **251**, 1801 (2014).
- [58] K. V. Shanavas, *Phys. Rev. B* **93**, 045108 (2016).
- [59] K. Ishizaka, M. S. Bahramy, H. Murakawa, M. Sakano, T. Shimojima, T. Sonobe, K. Koizumi, S. Shin, H. Miyahara, A. Kimura, K. Miyamoto, T. Okuda, H. Namatame, M. Taniguchi, R. Arita, N. Nagaosa, K. Kobayashi, Y. Murakami, R. Kumai, Y. Kaneko, Y. Onose, and Y. Tokura, *Nat. Mater.* **10**, 521 (2011).
- [60] S. LaShell, B. A. McDougall, and E. Jensen, *Phys. Rev. Lett.* **77**, 3419 (1996).
- [61] Z. Zhong, A. Tóth, and K. Held, *Phys. Rev. B* **87**, 161102(R) (2013).
- [62] H. Nakamura, T. Koga, and T. Kimura, *Phys. Rev. Lett.* **108**, 206601 (2012).
- [63] W. Lin, L. Li, F. Doğan, C. Li, H. Rotella, X. Yu, B. Zhang, Y. Li, W. S. Lew, S. Wang, W. Prellier, S. J. Pennycook, J. Chen, Z. Zhong, A. Manchon, and T. Wu, *Nat. Commun.* **10**, 3052 (2019).
- [64] Y. Yang, M. Stengel, W. Ren, X. H. Yan, and L. Bellaiche, *Phys. Rev. B* **86**, 144114 (2012).
- [65] C. Paillard, S. Prokhorenko, and L. Bellaiche, *Npj Comput. Mater.* **5**, 1 (2019).
- [66] A. Skierkowski and J. A. Majewski, *Acta Phys. Pol. A* **112**, 455 (2007).
- [67] R. D. King-Smith and D. Vanderbilt, *Phys. Rev. B* **47**, 1651 (1993).
- [68] L. Sun, Y. Chen, W. Ma, L. Wang, T. Yu, M. Zhang, and N. Ming, *Appl. Phys. Lett.* **68**, 3728 (1996).
- [69] J. Íñiguez, D. Vanderbilt, and L. Bellaiche, *Phys. Rev. B* **67**, 224107 (2003).